UV-ray irradiation never causes amorphization of crystalline CO_2: A transmission electron microscopy study

Masashi Tsuge[a,*], Thanh Nguyen[a], Yasuhiro Oba[a], Tetsuya Hama[b], Akira Kouchi[a], Naoki Watanabe[a]

[a] *Institute of Low Temperature Science, Hokkaido University, Sapporo, Hokkaido 060-0819, Japan*

[b] *Komaba Institute for Science, The University of Tokyo, 308-1 Komaba, Meguro, Tokyo 153-8902, Japan*

* Corresponding author at: Kita-19, Nishi-8, Kita-ku, Sapporo 060-0819, Japan.
Telephone: +81-11-706-5474
E-mail address: tsuge@lowtem.hokudai.ac.jp (M. Tsuge)

Keywords: astrochemistry, cosmic ice, transmission electron microscopy, infrared spectroscopy

HIGHLIGHTS

- Crystallinity of CO_2 under UV-ray irradiation was directly observed by TEM
- Amorphization of crystalline CO_2 upon UV-ray irradiation was not observed
- Stronger UV-ray irradiation in IR experiments did not cause amorphization either
- UV-fluence expected in molecular clouds will not cause amorphization of CO_2 ice

GRAPHICAL ABSTRACT

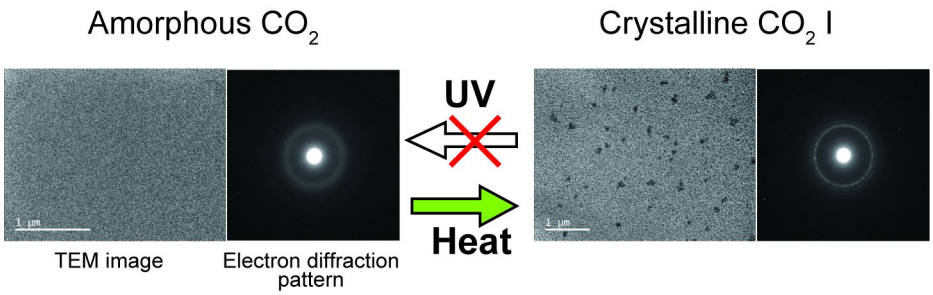

ABSTRACT

The Crystallinity of ices, amorphous and crystalline, can be altered not only by heat but also by irradiation of UV-rays or charged particles. In this work, the effect of UV-irradiation on the crystallinity of CO_2 ice was investigated by using a transmission electron microscope. A crystalline CO_2 ice was produced by annealing amorphous CO_2 ice. We found that UV-ray irradiation of CO_2 crystals at approximately 10 K does not cause amorphization in contrast to the reported amorphization of crystalline water ice below 70 K. We discuss the difference based on the expected UV photochemistry of CO_2 ice.

1. Introduction

The crystallinity of ices, amorphous or crystalline, in icy grains and the surface of icy bodies that exist in space are important because it provides information on their thermal history. It had been widely accepted that amorphous H_2O ice is formed at low temperatures and crystalline H_2O ice at higher temperatures [1]. However, the crystallinity of ices formed by the condensation of H_2O vapor could be determined by the temperature and deposition rate [2,3]. Furthermore, the time scale of crystallization of amorphous H_2O ice depends on the observation temperature [2,4,5].

It had been implicitly assumed until 1980s that the phase transition from amorphous H_2O ice to crystalline H_2O ice (ice I) was irreversible, and that from ice I to amorphous H_2O ice never occurred. However, the irradiation with UV-rays [6,7], electron beam [8,9] and other high-energy particle [10,11] causes the amorphization of ice I crystal at temperatures below ~70 K. These processes should be considered to evaluate the thermal history of ices because UV-rays and other particle irradiation hide the high-temperature history of ices. Although the amorphization of H_2O ice has been extensively investigated [5,12], the detailed mechanism of amorphization, which should involve the dissociation of H_2O molecules, has not been clarified.

Because CO_2 and CO are abundant ice components following H_2O, the crystallinity of CO_2 and CO is essential to discuss the thermal history of ices at lower temperatures in space. However, there have been few reliable works on the crystallinity of these ices, especially the formation of amorphous CO_2. Gerakines and Hudson noted that CO_2 solid used in past studies were not pure amorphous CO_2 but crystalline or mixture of amorphous and crystalline CO_2 [13]. Only Escribano et al. [14] and Gerakines and Hudson [13] succeeded in making pure amorphous CO_2. On the other hand, Baratta and Palumbo [15] and He and Vidali [16] claimed that the band shape that had been attributed to amorphous CO_2 is induced by a small amount of water incorporated into the CO_2 ice. Nevertheless, we note that the discussion on crystallinity has been done mostly without direct evidence. Among these studies, Escribano et al. [14] developed theoretical models to reproduce observed spectra. Mangan et al. used the X-ray diffraction method to show that vapor-deposited solid CO_2 at temperatures of 80–130 K was crystalline CO_2, CO_2 I [17]. It is noted here that crystalline polymorphs are usually distinguished using Roman numerals (e.g., CO_2 I, ice IX) or Greek letters (e.g., α-CO, β-quartz). Kouchi et al. experimentally demonstrated using transmission electron

microscopy that amorphous CO and CO_2 could be formed by vapor-deposition on amorphous H_2O ice at temperatures below 18 and 50 K, respectively [18]. They also showed that crystalline forms, α-CO and CO_2 I, were formed at temperatures higher than those temperatures. Kouchi showed by reflection electron diffraction method that amorphous CO crystallized at approximately 20 K to form α-CO [19].

For CO_2 and CO, there has been no investigation on the amorphization of their crystals by the irradiation with UV-rays or high-energy charged particles. It is highly desirable to verify the possibility whether amorphization will occur because of the irradiation. Because CO is hardly dissociated at wavelengths of UV-rays generated in molecular clouds, we focus on CO_2 in this study. Using transmission electron microscopy and infrared spectroscopy, we have performed in situ observation of CO_2 crystals and amorphous CO_2 upon UV-ray irradiation.

2. Experimental

2.1. Transmission electron microscopy

We used an ultrahigh vacuum transmission electron microscope (UHV-TEM) (JEOL, JEM-2100VL) for the in situ observation of the irradiation process [18,20,21]. The UHV-TEM was evacuated by ion pumps and Ti-sublimation pumps. The pressure measured in the region between the TEM column and the ion pump was 1×10^{-6} Pa. Since the specimen is surrounded by a liquid-N_2 shroud, the pressure near the specimen may be lower than 1×10^{-6} Pa because of the deposition of residual water vapor to the shroud. For sample cooling, we used a liquid He cooling holder (Gatan, ULTST). We used a 5-nm thick nonporous amorphous Si film (SiMPore Inc., US100-A05Q33) for a substrate of sample deposition. The UHV-TEM has three ports directed at the sample surface with an incident angle of 55°. One of the ports is used for CO_2 deposition through a Ti tube (0.4 mm inner diameter) and another for UV-irradiation. A 30-W D_2 lamp (Hamamatsu, L7293), which is equipped with an MgF_2 window and emits photons in the range of 115–400 nm, was used as a UV source. The lamp was directly connected to the vacuum port. The UV photon flux was measured using another vacuum chamber with Si-photodiode (IRD, AXUV-100G) to be ~2×10^{13} photons cm^{-2} s^{-1} before setting the lamp to TEM. UV-rays from the lamp equipped to TEM were collimated using a mirror-finished pure Al-collimator, which affects the actual UV flux at the sample position in TEM.

First, ~20-nm-thick amorphous CO_2 was deposited at 10 K with a deposition rate of ~1 nm min^{-1}, since Gerakines and Hudson report that amorphous CO_2 can be formed at the deposition rate below 1.7 nm min^{-1} [13]. The thickness of the CO_2 layer was measured following the method described by Kouchi et al. [18]. Then, amorphous CO_2 was crystalized by annealing at 60 K for 10 min. Crystalline CO_2 was subsequently cooled to 10 K and irradiated with UV-rays. We observed the entire process using TEM. To avoid electron beam damage, a low-dose technique has been applied following Tachibana et al. [21]: low magnification (×25000–50000), 80 kV accelerating voltage, and an electron beam density of 2–6 × 10^{-3} electrons $Å^{-2}$. Thus, we observed TEM images and electron diffraction patterns using a CCD camera (Gatan, ES500W). All electron diffraction patterns were taken in the 700-nm-diameter circular region of the central part of TEM images.

2.2. Infrared spectroscopy

We performed the following experiments for a longer duration using a stronger UV source. The experimental apparatus comprised a main ultrahigh vacuum chamber (base pressure < 2 × 10^{-7} Pa), a Si(111) substrate (40 mm × 40 mm × 1 mm) mounted on the cold head of a closed-cycle He refrigerator (Sumitomo Heavy Industries, RDK-101D), and a Fourier transform infrared spectrometer (FT-IR) (Thermo Fisher Scientific, Nicolet iS50). CO_2 gas (Air Water, 99.999%) was introduced onto the Si substrate at 8 K by background deposition, typically for 90 min at 8.9 × 10^{-6} Pa. The pressure was measured using a crystal ion gauge (Canon Anelva, M-336MX) and calculated using the gas correction factor for CO_2 (1.35) [22]. This corresponds to the flux of 2.0 × 10^{13} molecules cm^{-2} s^{-1}, and the deposited amount of CO_2 was estimated as 1.1 × 10^{17} molecules cm^{-2}.

Because we used a relatively slower deposition rate of CO_2, co-adsorption of background H_2O cannot be avoided. The partial pressures of background gasses were not determined in these experiments, but the dominant residual gas at such an ultrahigh vacuum condition should normally be hydrogen. Even we admit that the background pressure was dominated by water, the number of water molecules landing on the surface is less than 1 × 10^{15} molecules cm^{-2}. Therefore, the upper limit of H_2O/CO_2 ratio will be 1/100. At such dilution, almost all the CO_2 molecules in ice sample interact with other CO_2 molecules but not with H_2O, and one does not expect the change in the spectral

shape of CO_2 band. Moreover, such a small amount of H_2O should not affect the UV-induced processes investigated in this paper. He and Vidali demonstrated that the deposition of H_2O/CO_2 = 1/10 induces the spectral change of CO_2 band [16], but the H_2O/CO_2 is so high, as compared to present experimental conditions, that most of CO_2 might interact with H_2O molecule.

The prepared solid CO_2 sample was warmed to 60 K at a rate of 4 K min^{-1} for crystallization, and the crystalline CO_2 was cooled to 8 K for UV-irradiation using a 150-W D_2 lamp (Hamamatsu, L11798). The UV photon flux measured by the Si-photodiode was ~3×10^{14} photons cm^{-2} s^{-1}. The CO_2 samples were monitored in situ by the FT-IR in transmission geometry. The angles of incidence were 45° for UV-radiation from the D_2 lamp and IR light from the FT-IR due to the orthogonal configuration of the two vacuum ports in the chamber. For IR spectral measurements, the s-polarized IR light was employed to retrieve the pure transverse optic energy loss function from a sample without a contribution of longitudinal optic energy loss function [14]. Hence, the s-polarized transmission spectra can be directly compared to the normal incidence transmission spectrum of solid CO_2 previously reported in the literature [13,23]. Spectra were accumulated 100 times with a resolution of 4 cm^{-1}.

3. Results

3.1. TEM observation

Figure 1 shows the TEM images and electron diffraction patterns observed during UV irradiation experiments. CO_2 deposited at 10 K was amorphous (Figure 1a). After 10-min heating at 60 K, amorphous CO_2 completely crystallized to form CO_2 I crystals (Figure 1b). This is the first direct identification of crystalline structure of CO_2 formed by the crystallization of amorphous CO_2. The grain size distribution is bimodal with large crystals of 100–200 nm in diameter (black images in Figure 1b) and smaller crystals (gray images). After 35 min of UV-irradiation (UV fluence ~4×10^{16} photons cm^{-2}), we did not observe any textural and crystalline structure change (Figure 1c), which shows that CO_2 I crystals are not amorphized by UV-rays. As demonstrated for crystalline H_2O ice [7], the occurrence of UV-ray-induced amorphization process should be clearly seen as a change in electron-diffraction patterns.

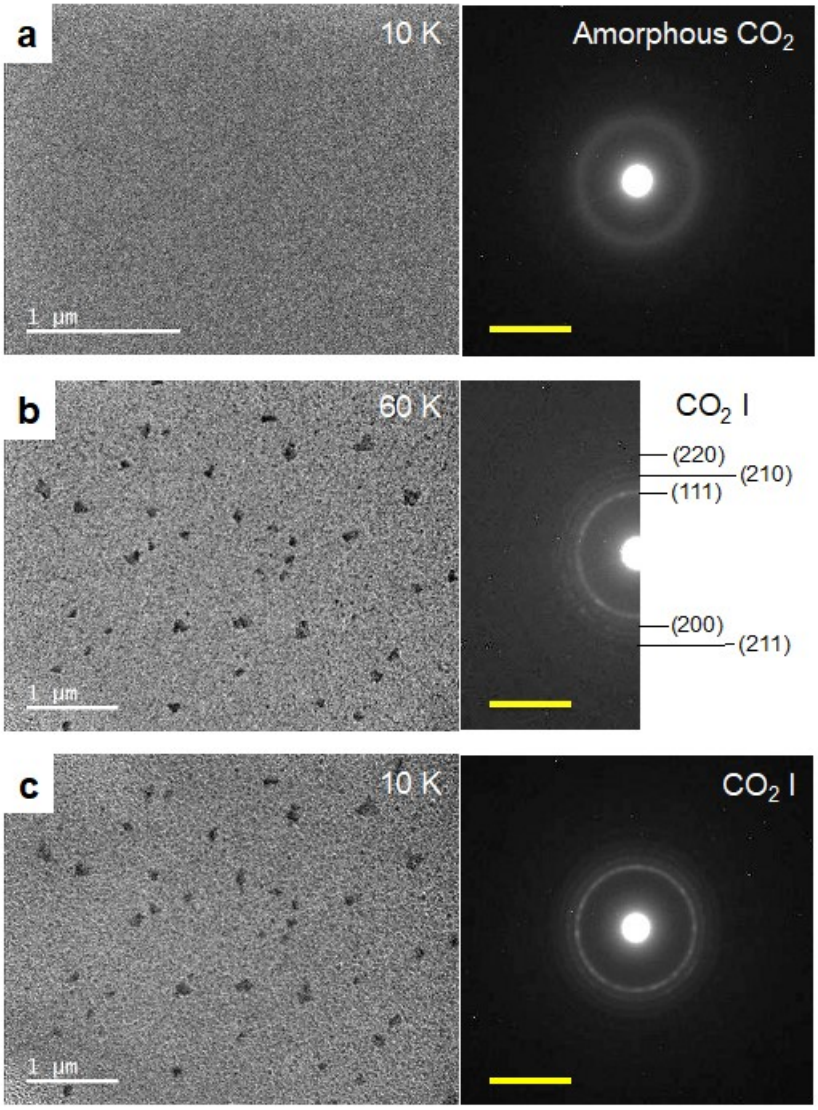

Figure 1. TEM observation of the UV irradiation experiment: (a) Amorphous CO_2 deposited on amorphous Si film at 10 K, (b) Crystallized CO_2 by 10 min of annealing at 60 K, and (c) 35-min UV-irradiated CO_2 at 10 K. The corresponding electron diffraction patterns are attached to the respective TEM images. The scale bars in electron diffraction patterns are 5 nm^{-1}.
(color on the WEB)

We also evaluated the effect of the electron beam of TEM. The stronger electron beam of ~10 electrons $Å^{-2}$ was applied for TEM measurement. Figure 2a shows the

TEM image and electron diffraction pattern immediately after starting the focused beam irradiation. After 22-min irradiation, most CO_2 I crystals have been sputtered as shown in Figure 2b. The roughly estimated sputtering rate of CO_2 I was ~<1 nm min^{-1}, which corresponded to the sputtering yield of 10^{-3} molecules $electron^{-1}$. However, the electron diffraction pattern clearly shows that remnant CO_2 was crystalline. Thus, CO_2 I crystal shows strong resistance against both UV-rays and electron beam.

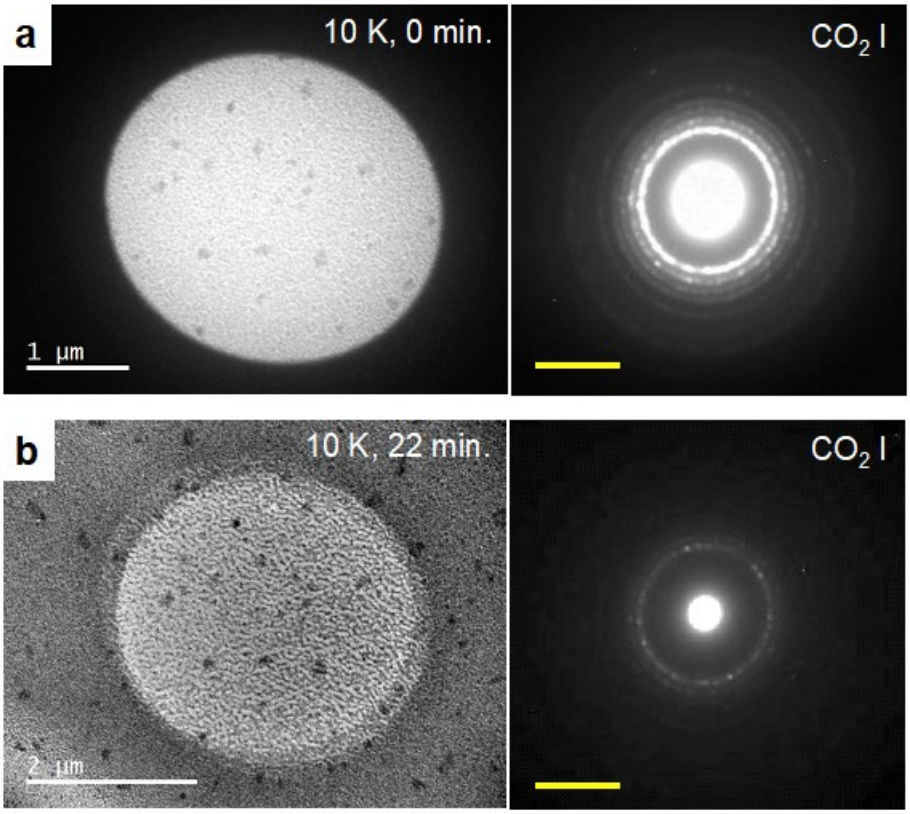

Figure 2. TEM images and corresponding electron diffraction patterns upon 80-kV electron beam irradiation: (a) immediately after starting irradiation and (b) after 22 min of irradiation. The electron beam was focused to 3-μm diameter (bright circle in a). The TEM image and electron diffraction pattern in (a) and (b) were taken using a strong electron beam of ~10 electrons $Å^{-2}$ and a weak electron beam of ~2 × 10^{-3} electrons $Å^{-2}$, respectively. The scale bars in electron diffraction patterns are 5 nm^{-1}.
(color on the WEB)

3.2 IR spectroscopy

To complement the relatively small UV flux used in TEM experiments, we performed additional experiments using IR spectroscopy with the higher UV fluence which is equivalent to that for >10^7 years in molecular clouds. We note that the interpretation of spectral shape of CO_2, which has been extensively debated in literature, is out of the scope of this paper. Figure 3 shows the IR spectra of a solid CO_2 sample in the ν_3 (antisymmetric stretching) region and in the $\nu_1 + \nu_3$ region. In the ν_3 region, the spectrum after deposition (trace a) shows an asymmetric band peaking near 2333 cm^{-1}, which is consistent with the spectral shape reported for amorphous CO_2 [13]. Based on the TEM observation that slow CO_2 deposition yields amorphous CO_2 ice (Figure 1(a)), we attribute the observed band to amorphous CO_2 ice. The $\nu_1 + \nu_3$ band of amorphous CO_2 ice was observed near 3704 cm^{-1}, consistent with the position reported by He and Vidali [16]. The amorphous CO_2 sample was annealed at 60 K to obtain crystalline CO_2 (trace b), which shows a more symmetric bands centering at 2342 cm^{-1} in the ν_3 region and at 3708 cm^{-1} in the $\nu_1 + \nu_3$ region; the latter band has been assigned to crystalline CO_2 [16]. During warm-up, an obvious shift in peak positions from 2333 to 2342 cm^{-1} was observed at temperatures above 35 K. Correlated changes in the ν_3 and $\nu_1 + \nu_3$ regions upon annealing will be presented later. Integrated absorbance did not change upon crystallization, indicating that band strengths are more or less the same for amorphous and crystalline CO_2. The crystalline CO_2 was irradiated at 8 K with the 150-W D_2 lamp for 20 min (UV fluence 3–4 × 10^{17} photons cm^{-2}), and the spectrum measured after irradiation was shown as trace c. After this process, the peak position was unchanged, which confirms that UV-induced amorphization did not occur even when crystalline CO_2 were irradiated with stronger UV-rays for longer duration. The decrease in integrated absorbance from 1.251 to 1.153 cm^{-1} (~10% decrease) guarantees that the applied UV fluence was sufficiently large for photoinduced processes of CO_2 to occur. Longer UV irradiation induced a slight decrease of CO_2 (~15% decrease after 90-min irradiation). The peaks of photoproduct were observed at 2140, 2044, and 1044 cm^{-1}, which are thought to originate from CO, CO_3, and O_3, respectively [24]. Although a precise quantitative analysis on photodissociation reactions is not possible due to the lack of information on the absorption coefficients of these species in solid CO_2, the

estimated column densities of products comparable to the decrease of CO_2 indicate that the photodissociation instead of photodesorption contributes to the decrease of CO_2. The absence of UV-ray-induced amorphization can also be recognized in the IR spectra reported by Martín-Doménech et al. [25]. Although these authors did not mention the crystallinity of their solid CO_2 sample, their IR spectra indicate that mixture of amorphous and crystalline CO_2 sample became crystalline CO_2 upon UV-ray irradiation.

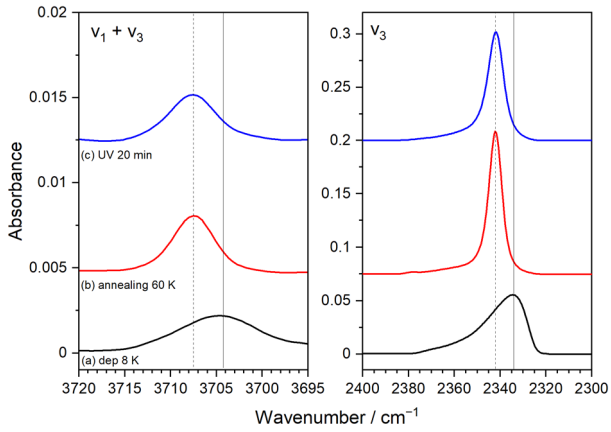

Figure 3. Infrared spectra of solid CO_2 in the $\nu_1 + \nu_3$ region 3720–3695 cm^{-1} and in the ν_3 region 2400–2300 cm^{-1}. (a) After deposition at 8 K. (b) After annealing at 60 K for 10 min. The warming-up and cooling-down rate was 4 K min^{-1}. (c) After irradiation by the D_2 lamp for 20 min. All spectra were measured at 8 K. Peak positions for amorphous CO_2 at 3704 and 2333 cm^{-1} are indicated with solid lines and those for crystalline CO_2 at 3708 and 2342 cm^{-1} are indicated with dashed lines.
(color on the WEB)

He and Vidali presented a method to investigate a degree of crystallinity in CO_2 sample by using the $\nu_1 + \nu_3$ combination band since determining the degree of crystallinity from the spectral shape of the ν_3 band in IR spectra acquired with the reflection absorption configuration is difficult [16]. We found that, in the IR spectra measured with transmission configuration, the peak position of ν_3 band gradually shifts

from 2333 to 2342 cm^{-1} as crystallization proceeds and the alternation correlates with the shape change of the $\nu_1 + \nu_3$ combination band (see Figure 4), for which 3704 and 3708 cm^{-1} peaks have been attributed to amorphous and crystalline CO_2, respectively. Therefore, when using IR spectra measured with transmission configuration, we deduce that the IR band of ν_3 mode is also representative of crystallinity.

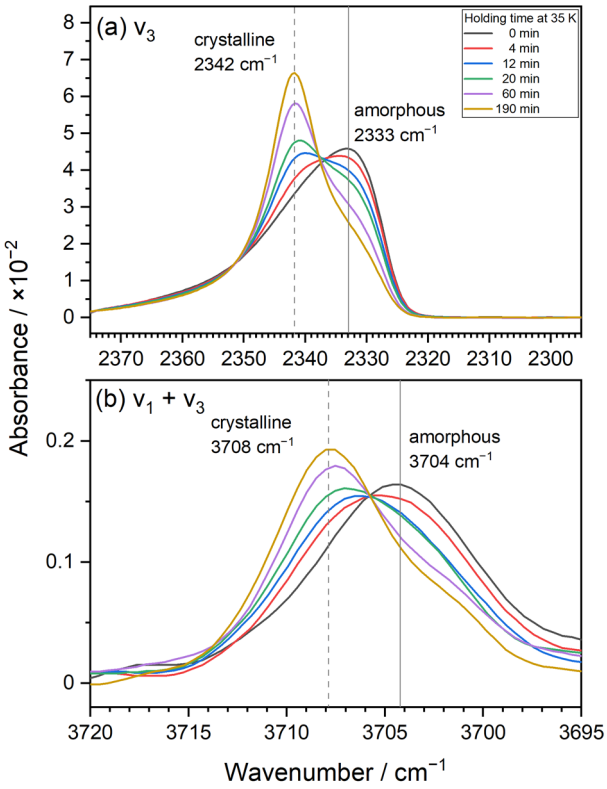

Figure 4. Infrared spectra of solid CO_2 in regions (A) 2375–2950 and (B) 3720–3695 cm^{-1}. The sample was deposited at 8 K and annealed to 35 K. Just after reaching 35 K, IR measurements were started. The spectra measured after 0, 4, 12, 20, 60, and 190 min are presented in different colors. Peak positions for amorphous and crystalline CO_2 are indicated with solid and dashed lines, respectively.
(color on the WEB)

4. Discussion

4.1. Why does CO_2 I crystal not amorphize?

As mentioned earlier, the amorphization of crystalline H_2O ice by UV-irradiation has been demonstrated [6,7]. In contrast, we found that UV-ray irradiation does not induce the amorphization of crystalline CO_2. Below, we discuss possible UV-induced processes in CO_2 solid.

CO_2 molecule is decomposed by UV-rays [26]:

$$CO_2 + UV \rightarrow CO + O\ (^1D),\ O\ (^3P). \quad (1)$$

The formation of O (^{1}D) is a major spin-allowed path. Although the dissociation to O (^{3}P) is spin-forbidden, this channel was clearly observed in the gas phase [26]. The produced energetic O would not escape from the CO_2 I lattice because CO_2 I is compact face-centered cubic crystal. When an O (^{1}D) atom is produced in reaction (1), several reactions are expected.

$$O\ (^1D) + CO \rightarrow CO_2;\ \Delta E = -167\ \text{kcal mol}^{-1}\ [27] \quad (2)$$

$$O\ (^1D) + CO_2 \rightarrow CO_3;\ \Delta E = -197\ \text{kcal mol}^{-1}\ [28] \quad (3)$$

$$O\ (^1D) + CO_2 \rightarrow O\ (^3P) + CO_2;\ \Delta E = -45\ \text{kcal mol}^{-1}\ [29] \quad (4)$$

In the UV-ray irradiation experiments, the CO_2 depletion saturated after long irradiation (90 min, UV fluence ~1.5×10^{18} photons cm^{-2}), which suggests that CO_2 destruction (e.g., reaction (1)) and formation (reaction (2)) are well balanced at this moment. The occurrence of reactions (1) and (3) is inferred from the IR spectra of UV-ray-irradiated solid CO_2, where products CO and CO_3 were observed. Even if an O (^{1}D) atom is quenched to O (^{3}P) in reaction (4), the resultant O (^{3}P) atom can react with CO:

$$O\ (^3P) + CO \rightarrow CO_2;\ \Delta E = -22\ \text{kcal mol}^{-1}\ [30] \quad (5)$$

Because of the energy barrier, which is ~4 kcal mol^{-1} in the gas phase, this reaction requires energetic O (^{3}P) atom and/or CO molecule. Nevertheless, the occurrence of reaction (5) in irradiated solid CO_2 has been reported in the literature [31] and is consistent with theoretical predictions [30].

Reactions (1)-(5) are exothermic reactions, which can heat the region where they occur. In other words, the occurrence of these reactions converts the energy of UV-rays into thermal energy. Because the crystalline structure is energetically more stable than the amorphous structure, these thermal energies should induce crystallization. The photolysis of CO_2, which is reaction (1), is considered an amorphization process, since it creates a defect in the CO_2 lattice. Thus, a competition between this UV-induced amorphization and the crystallization induced by heat produced in reactions (1)-(5) is

important to determine the fate of UV-ray-irradiated CO_2 solid. The experimental results strongly suggest that the latter processes are significant in the CO_2 case.

Since the cosmic-ray-induced UV flux in molecular clouds is ~10^3 photons cm^{-2} s^{-1}, one second of UV irradiation in the TEM and IR experiments corresponds to ~10^3 and 10^4 years of UV irradiation in molecular clouds, respectively. We did not observe any amorphization even after 90 min of irradiation in the IR experiment, which corresponds to 5×10^7 years in molecular clouds. Therefore, our results indicate that the UV-induced amorphization of CO_2 crystal is unlikely to occur in molecular clouds.

Similarly, UV-ray-induced chemical reactions are expected in crystalline H_2O ice; i.e., exothermic reactions such as $H + OH \rightarrow H_2O$ and $H + H \rightarrow H_2$ would occur following the decomposition by UV-ray, $H_2O + UV \rightarrow H + OH$ or other products. However, it has been reported that UV-ray-induced amorphization of crystalline H_2O ice occurs at temperature below 70 K [7]. In addition, preliminary experiments reveal that the UV-ray-induced crystallization of amorphous H_2O occurs in the temperature range of 70–100 K (Kouchi et al. unpublished work). These different behaviors of CO_2 solid and H_2O ice to UV-ray irradiation might be related to the dissipation rate of reaction heats. Famá et al. [12] discussed the ion-bombardment-induced amorphization of crystalline H_2O based on a thermal spike model, which was modified based on Szenes's model [32], and they suggested that the very fast cooling of a transient liquid track produced by each ion led to amorphization. Analogously, we deduce that the cooling of locally heated CO_2 molecules is slower than the H_2O case, so that CO_2 molecules in this region have sufficient time to return to the original positions. This local thermal dissipation process might not be scaled by bulk property of solids, e.g., thermal conductivity. To gain further insight into the difference between H_2O ice and CO_2 solid, simulations including molecular level dynamics will be required, and they are out of the scope of this paper.

4.2. The absence of amorphous CO_2 in molecular clouds

Escribano et al. suggested the absence of amorphous CO_2 in space based on the comparison of 2343 cm^{-1} band towards Elias 16 with the laboratory spectrum [14]. They simply assumed that the crystallization temperature of amorphous CO_2 in molecular clouds was identical to that observed in the laboratory, which is approximately 25 K. However, the crystallization temperature greatly depends on the

time scale of experimental observation as demonstrated for amorphous H_2O [4]. Therefore, it is reasonable to assume that crystallization temperature of amorphous CO_2 in molecular clouds is much lower than 25 K. Recently, from the fitting of the 15-μm band of Q21-1 using bands of crystalline CO_2 and amorphous CO_2, Gerakines and Hudson suggested that up to ~9% of CO_2 might be amorphous [13]. However, the validity of their fitting requires further assessment.

Here, we will discuss some factors that control the crystallinity of CO_2. First, we assume that CO_2 molecules formed by the following grain surface reaction [33,34] result in an amorphous form regardless of the reaction heat:

$$CO + OH \rightarrow \textit{cis}\text{-}HOCO^* \rightarrow \textit{trans}\text{-}HOCO^* \rightarrow CO_2 + H;\ \Delta E = -23\ \text{kcal mol}^{-1} \quad (6)$$

where asterisks indicate reaction intermediates. Crystalline CO_2 can be amorphized by the irradiation of high-energy particles, although we have no experimental evidence. Another possible crystallization mechanism of amorphous CO_2 is that crystallization might be promoted even at low temperature in molecular clouds. Because crystallization temperatures in the molecular cloud time scale are lower than those in the laboratory; crystallization temperatures in the time scale of 10^6 years might be lower than 20 K. Actually, Kouchi et al. (in prep.) estimated the time scale of crystallization at 15 K to be 10^6 years. Although the above discussion is still preliminary due to the lack of quantitative data, we suggest that the crystallization of amorphous CO_2 might proceed even in low-temperature molecular clouds, if amorphous CO_2 is formed at first.

Finally, we consider the direct formation of crystalline CO_2. a) Chemical desorption is proposed as one of the nonthermal desorption mechanisms of molecules in low-temperature molecular clouds [35,36], and some experiments support this idea [37-39]. Thus, CO_2 formed by reaction (6) has sufficient energy to diffuse and cause crystallization, since the activation energy of surface diffusion is 0.3-0.5 of the desorption energy. b) Local heating by reaction (6) could induce the crystallization.

Declaration of Competing Interest

The authors declare that they have no known competing financial interests or personal relationships that could have appeared to influence the work reported in this paper.

Acknowledgments

This work was supported by the Japan Society for the Promotion of Science Grants-in-Aid for Scientific Research (KAKENHI; grant numbers JP16H04072, JP17H06087, JP18K03717, JP18H01262, JP19K22901, and JP19K23449).

REFERENCES

[1] P.V. Hobbs, Ice Physics, Oxford University Press, Clarendon, Oxford, 1974.

[2] A. Kouchi, T. Yamamoto, T. Kozasa, T. Kuroda, J.M. Greenberg, Astron. Astrophys. 290 (1994) 1009.

[3] F.J. Ciesla, Astrophys. J. Lett. 784 (2014) L1.

[4] P. Jenniskens, D.F. Blake, Astrophys. J. 473 (1996) 1104.

[5] R.A. Baragiola, Planet. Space Sci. 51 (2003) 953.

[6] G. Leto, G.A. Baratta, Astron. Astrophys. 397 (2003) 7.

[7] A. Kouchi, T. Kuroda, Nature 344 (1990) 134.

[8] H.G. Heide, Ultramicroscopy 14 (1984) 271.

[9] H.G. Heide, E. Zeitler, Ultramicroscopy 16 (1985) 151.

[10] G. Strazzulla, G.A. Baratta, G. Leto, G. Foti, Europhys. Lett. 18 (1992) 517.

[11] M.H. Moore, R.L. Hudson, Astrophys. J. 401 (1992) 353.

[12] M. Famá, M.J. Loeffler, U. Raut, R.A. Baragiola, Icarus 207 (2010) 314.

[13] P.A. Gerakines, R.L. Hudson, Astrophys. J. Lett. 808 (2015) L40.

[14] R.M. Escribano, G.M. Muñoz Caro, G.A. Cruz-Diaz, Y. Rodríguez-Lazcano, B. Maté, Proc. Natl. Acad. Sci. 110 (2013) 12899.

[15] G.A. Baratta, M.E. Palumbo, Astron. Astrophys. 608 (2017) A81.

[16] J. He, G. Vidali, Monthy Notices of the Royal Astronomical Society 473 (2017) 860.

[17] T.P. Mangan, C.G. Salzmann, J.M.C. Plane, B.J. Murray, Icarus 294 (2017) 201.

[18] A. Kouchi, K. Furuya, T. Hama, T. Chigai, T. Kozasa, N. Watanabe, Astrophys. J. Lett. 891 (2020) L22.

[19] A. Kouchi, J. Cryst. Growth 99 (1990) 1220.

[20] A. Kouchi, T. Hama, Y. Kimura, H. Hidaka, R. Escribano, N.

Watanabe, Chem. Phys. Lett. 658 (2016) 287.
[21] S. Tachibana, A. Kouchi, T. Hama, Y. Oba, L. Piani, I. Sugawara, Y. Endo, H. Hidaka, Y. Kimura, K.-i. Murata, H. Yurimoto, N. Watanabe, Sci. Adv. 3 (2017) eaao2538.
[22] K. Nakayama, H. Hojo, Jpn. J. Appl. Phys. Suppl. 2 (1974) 113.
[23] T. Hasegawa, Quantitative Infrared Spectroscopy for Understanding of a Condensed Matter, Splinger Japan, Japan, 2017.
[24] P.A. Gerakines, W.A. Schutte, P. Ehrenfreund, Astron. Astrophys. 312 (1996) 289.
[25] R. Martín-Doménech, J. Manzano-Santamaría, G.M. Muñoz Caro, G.A. Cruz-Díaz, Y.-J. Chen, V.J. Herrero, I. Tanarro, Astron. Astrophys. 584 (2015) A14.
[26] S. Yu, D. Yuan, W. Chen, J. Zhou, X. Yang, X. Wang, J. Chem. Phys. 151 (2019) 214306.
[27] D. Talbi, G.S. Chandler, A.L. Rohl, Chem. Phys. 320 (2006) 214.
[28] C.J. Bennett, C. Jamieson, A.M. Mebel, R.I. Kaiser, Phys. Chem. Chem. Phys. 6 (2004) 735.
[29] H. Okabe, Photochemistry of Small Molecules, Wiley, New York, 1978.
[30] M. Braunstein, J.W. Duff, J. Chem. Phys. 112 (2000) 2736.
[31] U. Raut, R.A. Baragiola, Astrophys. J. Lett. 737 (2011) L14.
[32] G. Szenes, Phys. Rev. B 51 (1995) 8026.
[33] H.-G. Yu, J.T. Muckerman, T.J. Sears, Chem. Phys. Lett. 349 (2001) 547.
[34] Y. Oba, N. Watanabe, A. Kouchi, T. Hama, V. Pirronello, Astrophys. J. Lett. 712 (2010) L174.
[35] D.A. Williams, Astrophys. J. 151 (1968) 935.
[36] R.T. Garrod, V. Wakelam, E. Herbst, Astron. Astrophys. 467 (2007) 1103.
[37] M. Minissale, F. Dulieu, S. Cazaux, S. Hocuk, Astron. Astrophys. 585 (2016) A24.
[38] K.J. Chuang, G. Fedoseev, D. Qasim, S. Ioppolo, E.F.v. Dishoeck, H. Linnartz, Astrophys. J. 853 (2018) 102.
[39] Y. Oba, T. Tomaru, T. Lamberts, A. Kouchi, N. Watanabe, Nat. Astron.

2 (2018) 228.